Metal-Free Electrocatalysts

DOI: 10.1002/ange.201100170

Graphene-Based Carbon Nitride Nanosheets as Efficient Metal-Free Electrocatalysts for Oxygen Reduction Reactions**

Shubin Yang, Xinliang Feng, Xinchen Wang, and Klaus Müllen**

In memory of Emanuel Vogel

Highly active catalysts for the oxygen reduction reactions (ORR) have long been regarded as a key to optimize the performance of fuel cells because of the kinetic sluggishness of ORR with a complex four-electron transfer process.[1] Although platinum-based catalysts for ORR were developed for the Apollo lunar mission as early as the 1960s, their large-scale commercial applications have been precluded by high costs and scarcity of platinum.[2] Therefore, numerous efforts have been devoted to reduce or substitute Pt-based catalysts by employing Pt-based alloys,[3] nonprecious metal catalysts,[4] enzymatic electrocatalysts,[5] or nitrogen-enriched carbonaceous materials.[1a,b,2a,6] Very recently, nitrogen-doped carbon nanotubes[1a] and mesoporous graphitic arrays[6a] have been proposed as potential metal-free catalysts for ORR because they not only exhibit excellent electrocatalytic activity but also possess the advantages of low costs, long durability, and environmental friendliness. Moreover, quantum mechanical calculations[7] and experimental investigations[6a,8] both reveal that the incorporation of nitrogen, especially the pyridinic or/and graphitic nitrogen in the carbon frameworks plays an essential role in the highly electrocatalytic activity for ORR. In this regard, carbon nitride (CN), a carbonaceous material that is enriched with a very high nitrogen content including both pyridinic and graphitic nitrogen moieties and that can be readily obtained through the pyrolysis of cyanamide,[9] melamine,[10] or ethylenediamine/carbon tetrachloride,[11] may serve as a potential metal-free catalyst for ORR. However, the low electrical conductivity ($<10^{-2}\,S\,cm^{-1}$) of CN materials constitutes a major obstacle for their application in fuel cells given that the electron transport in a CN electrode would be significantly hampered during the oxygen reduction process.[12]

Graphene, a monolayer of carbon atoms arranged in a honeycomb network, shows many intriguing properties such as superior electrical conductivity,[13] a large surface area,[14] excellent mechanical flexibility,[15] and high thermal/chemical stability.[16] To harness these unique properties, we have recently developed an efficient strategy for the fabrication of graphene-based sandwich-like nanosheets by using single-layer graphene as a template, thus providing numerous opportunities for applications of graphene-based nanocomposites.[17] Herein we demonstrate the successful fabrication of graphene-based carbon nitride (G–CN) nanosheets with individual dispersion of graphene between the nanosheets by a nanocasting technology. The typical synthesis protocol involves the employment of graphene-based mesoporous silica nanosheets (GM–silica) as a template and ethylenediamine and carbon tetrachloride as CN precursors. Remarkably, the resulting G–CN nanosheets not only possess a high nitrogen content, thin thicknesses, high surface areas, and large aspect ratios but also show enhanced electrical conductivity. Such unique features are favorable for the access of oxygen to the catalyst surface and can facilitate the rapid diffusion of electrons in the electrode during the oxygen-reduction process. As a consequence, the G–CN nanosheets exhibit an excellent electrocatalytic performance for ORR, including high electrocatalytic activity, long-term durability, and high selectivity, all of which are superior to those observed for CN sheets without graphene as well as for commercially available Pt–C catalysts.

As illustrated in Figure 1, graphene-oxide-based silica nanosheets were first fabricated by the hydrolysis of tetraethylorthosilicate on the surface of graphene oxide with the help of a cationic surfactant (cetyltrimethyl ammonium bromide, CTAB).[17] The resulting graphene-oxide-based silica nanosheets were then annealed at 800 °C under argon or air, respectively. Heating treatment under argon rendered the thermal reduction of graphene oxide to graphene and afforded the graphene-based mesoporous nanosheets as black powder (Figure S1 in the Supporting Information).[17] On the contrary, white mesoporous silica nanosheets were obtained in the presence of air because the graphene was completely burned off. Ethylenediamine and carbon tetrachloride were subsequently impregnated into the pores of the above mesoporous nanosheets and polymerized at 90 °C for 4 h. Further pyrolysis was carried out at 600, 800, and 1000 °C, respectively, for the formation of carbon nitride. Final etching of silica in 2 M NaOH solution generated CN nanosheets with

[*] Dr. S. Yang, Dr. X. Feng, Prof. Dr. K. Müllen
Max Planck Institute for Polymer Research
Ackermannweg 10, 55128 Mainz (Germany)
Fax: (+49) 6131-379-350
E-mail: feng@mpip-mainz.mpg.de
muellen@mpip-mainz.mpg.de
Dr. X. Wang
Max Planck Institute of Colloids and Interfaces
Research Campus Golm, 14424 Potsdam (Germany)

[**] This work was financially supported by the Max Planck Society through the program ENERCHEM, the German Science Foundation (Korean-German IRTG), DFG Priority Program SPP 1355, DFG MU 334/32-1, DFG Priority Program SPP 1459, BMBF LiBZ Project, and ESF Project GOSPEL (Ref Nr: 09-EuroGRAPHENE-FP-001). We also thank Prof. Markus Antonietti for helpful discussions.

Supporting information for this article is available on the WWW under http://dx.doi.org/10.1002/anie.201100170.

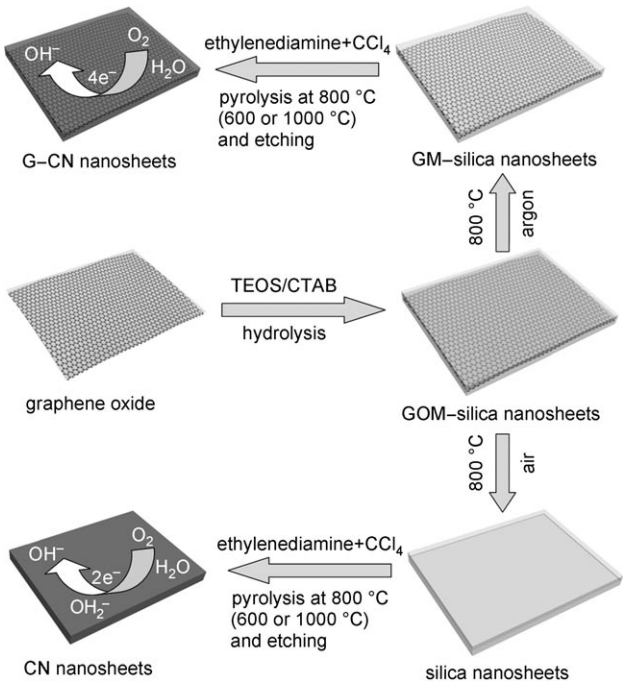

Figure 1. Fabrication of graphene-based carbon nitride (G–CN) and CN nanosheets for the ORR.

(G–CNX) and without (CNX) graphene; G and X represent the presence of graphene and the pyrolysis temperature, respectively.

The morphology and structure of G–CN nanosheets were investigated by means of TEM and field-emission scanning electron microscopy (FE-SEM). As indicated in Figure 2 and S2, large amounts of nanosheets in size from 200 nm to several micrometers and with a large aspect ratio can be produced. Obviously, such a morphology originates from the perfect replication of the GM–silica template. Although some of the G–CN nanosheets remain as planar as the GM–silica sheets, most of them become crumpled, possibly because of the shrinkage of the CN sample during the thermal treatment process or because of the intrinsic flexibility of CN materials. The 2D features of G–CN can be further confirmed by AFM analyses (Figure 2c) that reveal the uniform thickness of approximately 18 nm for ten different samples. It is worth noting that the thickness of G–CN nanosheets can be easily adjusted by choosing GM–silica nanosheets with various thicknesses as the template in our synthesis process. The typical TEM images (Figure 2b and S2b) in association with the XRD pattern (Figure S3) disclose the porous and amorphous nature of the G–CN nanosheets. A high Brunauer–Emmett–Teller (BET) surface area of up to 542 $m^2 g^{-1}$ is obtained on the basis of nitrogen adsorption–desorption analysis. This value is much higher than that of nonporous carbon nitride (5 $m^2 g^{-1}$)[12] and similar to that reported for mesoporous carbon nitride (505 $m^2 g^{-1}$).[11a] Moreover, the type-IV isotherm with pronounced adsorptions at medium and high relative pressures (0.4–0.9 P/P_o), demonstrates the existence of a large number of mesopores and micropores within the G–CN nanosheets (Figure 2d), which could be due to the replication of the mesoporous template and the continuous decomposition of CN precursors during thermal treatment.

X-ray photoelectron spectroscopy (XPS) measurements and elemental analysis were performed to probe the chemical composition and the content of nitrogen in the G–CN

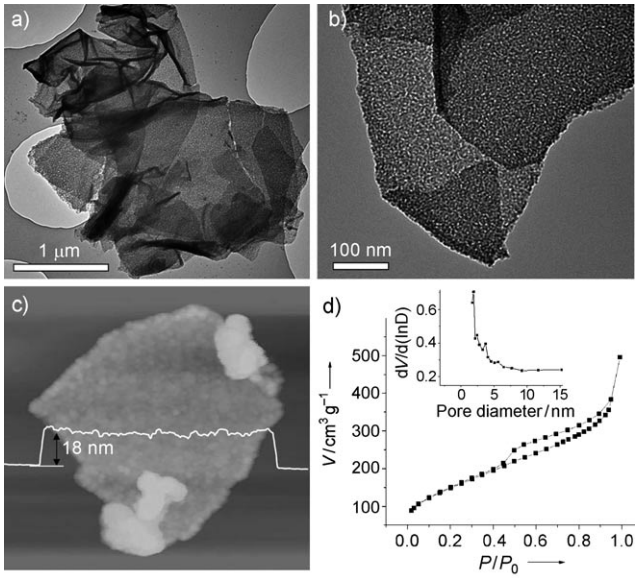

Figure 2. Typical a, b) TEM, and c) AFM images of G–CN nanosheets. d) Nitrogen adsorption/desorption isotherm of G–CN nanosheets (inset: pore-size distribution), demonstrating the mesoporous structure with a pore size < 5 nm and a BET surface area of 542 $m^2 g^{-1}$.

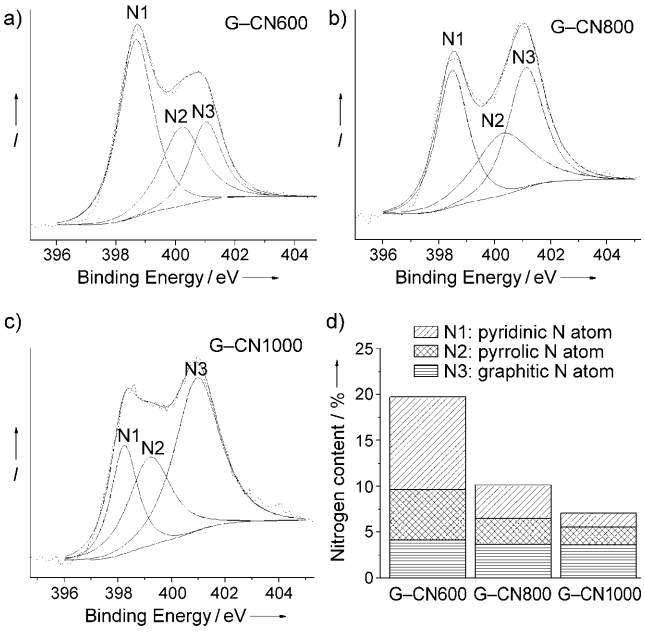

Figure 3. High-resolution N1s XPS spectra of a) G–CN600, b) G–CN 800, and c) G–CN 1000 nanosheets. The signals fit into three energy components centered around 398.0, 400.0, and 401.3 eV, and correspond to pyridinic N (N1), pyrrolic N (N2), and graphitic N (N3), respectively. d) The content of three nitrogen species (N1, N2, and N3) in G–CN nanosheets.

nanosheets. The survey scan spectra from XPS analysis reveal the presence of C1s, O1s, and N1s without any other impurities for all G–CN samples (Figure 3 and S4). The predominant C1s signals are centered at approximately 285.0 eV (graphite-like sp^2 carbon) and are asymmetric. This result is commonly observed for CN materials because of the dominant existence of C–N bonds in the matrix.[11] With an increase in pyrolysis temperature, the C1s signals shift to lower binding energy and their full width at half maximum becomes narrower (Figure S4b), thus indicating an enhanced degree of graphitization in the G–CN nanosheets. This finding can be further supported by Raman spectroscopy (Figure S5), in which the intensity of the G-peak at approximately 1589 cm^{-1} is slightly higher than that of the D-peak at approximately 1355 cm^{-1} with an increase in pyrolysis temperature. The presence of oxygen can be attributed to moisture, atmospheric O_2, or CO_2 adsorbed on G–CN nanosheets as well as the residual oxygen-containing groups (such as carbonyl groups, carboxyl groups, etc.) that remain at the edges or in the plane of reduced graphene. The complex N1s spectra can be further deconvoluted into three different signals with binding energies of 398.0, 400.0, and 401.3 eV that correspond to pyridinic N (N1), pyrrolic N (N2), and graphitic N (N3), respectively.[2a,6a] Remarkably, the shape of these three peaks significantly changes when the pyrolysis temperature is increased, thus suggesting that different amounts of N-bonding configurations are formed at different temperatures. In the case of G–CN600, pyridinic N is dominant, thus accounting for more than half of the overall N content (19%). When the pyrolysis temperature is increased to 800 and 1000 °C, the amount of graphitic N remains constant, whereas those of pyridinic N and pyrrolic N largely decrease, hence implying that these species are less stable at high temperatures. As a result, the overall nitrogen content of the G–CN nanosheets evidently decreases to 10 and 7% for G–CN800 and G–CN1000, respectively (Figure 3d). Thus, such different amounts of N-bonding configurations in G–CN samples must exert a large influence on their electrocatalytic performances for oxygen reduction (see below).

The electrocatalytic activity of G–CN nanosheets for ORR was first examined by cyclic voltammetry (CV) in 0.1 M KOH solution saturated with argon or oxygen. As shown in Figure 4a, featureless voltammetric currents within the potential range from −1.0 to +0.2 V are observed for G–CN800 in the argon-saturated solution. In contrast, a well-defined cathodic peak centered at −0.25 V emerges in the CV as the electrolyte solution is saturated with O_2, hence suggesting a pronounced electrocatalytic activity of G–CN800 for oxygen reduction. To evaluate the properties of a new electrocatalyst, the crossover effect should be considered because the fuel molecules such as methanol and glucose in the anode sometimes permeate through the polymer membrane to the cathode and seriously affect the performance of the cathode catalysts.[2a] Thus, the electrocatalytic sensitivity of G–CN800 and commercial Pt–C catalysts were measured against the electrooxidation of methanol in ORR. As shown in Figure 4b and Figure S6, a strong response is observed for the Pt–C catalyst in O_2-saturated 0.1 M KOH solution with 3 M methanol, whereas no noticeable response for G–CN800 is detected under the same testing conditions. Apparently, G–CN800 nanosheets exhibit a high selectivity for ORR with a remarkably good tolerance of crossover effects, thus being superior to the commercial Pt–C catalyst.

To gain further insight into the oxygen reduction reaction in G–CN nanosheets, rotating disk electrode (RDE) voltammetry was performed in O_2-saturated 0.1 M KOH solution at a scanning rate of 10 $mV s^{-1}$. For comparison, CN nanosheets without graphene were also investigated under the same conditions. It is striking that the onset potentials of all G–CN nanosheets are more positive than those of CN nanosheets

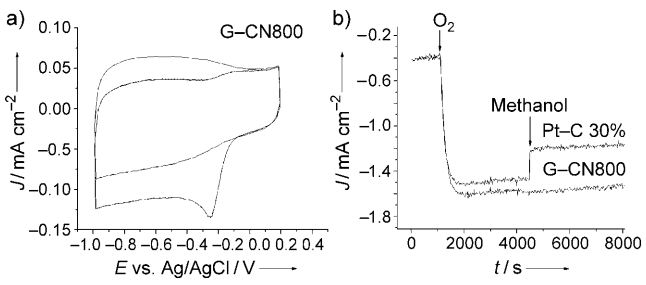

Figure 4. a) Cyclic voltammograms of G–CN800 at a scan rate of 100 $mV s^{-1}$ in O_2 (solid line; lower-lying curve) and Ar-saturated (solid line; higher-lying curve) 0.1 M KOH solution as well as O_2-saturated 0.1 M KOH solution with 3 M methanol (dashed line; the two lower-lying curves for the two O_2-saturated solutions are fully overlapped); b) Current–time (*I*–*t*) chronoamperometric responses at −0.25 V in O_2-saturated 0.1 M KOH on G–CN800 and Pt–C electrode (1600 rpm) followed by introduction of O_2 and methanol (0.3 M).

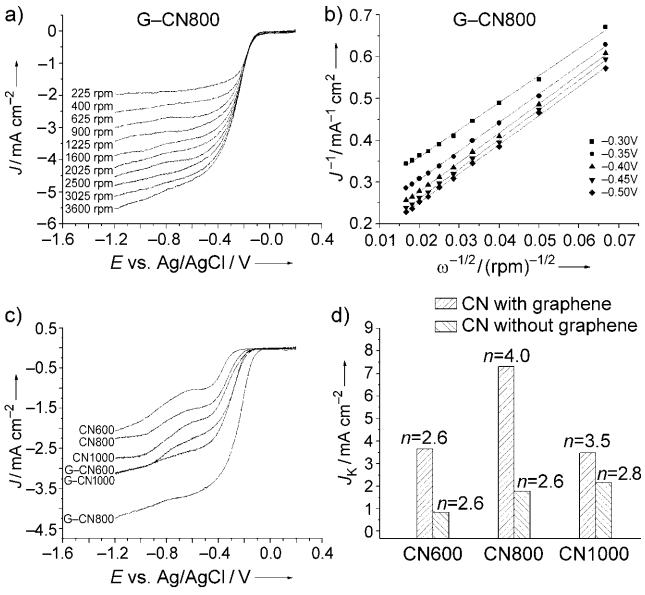

Figure 5. a) Rotating disk electrode (RDE) linear sweep voltammograms of G–CN800 in O_2-saturated 0.1 M KOH with various rotation rates at a scan rate of 5 $mV s^{-1}$. b) Koutecky–Levich plots of G–CN800 derived from RDE voltammograms in (a) at different electrode potentials. c) RDE voltammograms of G–CN and CN nanosheets at a rotation rate of 1600 rpm. The experimental conditions are the same as in (a). d) Electrochemical activity given as the kinetic-limiting current density (J_K) at −0.40 V for all G–CN and CN nanosheets.

without graphene (Figure 5c), hence suggesting that graphene in nanosheets significantly affects their electrocatalytical behavior and the overpotential of the overall electrodes. The exact kinetic parameters including electron transfer number (n) and kinetic current density (J_K) were analyzed on the basis of Koutecky–Levich equations[6a,18] (see the Supporting Information) and were summarized in Figure 5d. Remarkably enough, G–CN800 nanosheets exhibit a one step, four-electron transfer pathway with a high kinetic current density of 7.3 mA cm^{-2}. This value is four times higher than that of CN800 ($J_k = 1.8$ mA cm^{-2} at -0.40 V) and superior to that of commercially available Pt–C ($J_k = 5.4$ mA cm^{-2} at -0.40 V, Figure S7). In contrast, the CN nanosheets without graphene typically show a two-electron transfer pathway for ORR with low current densities ($J_k = 0.85$–2.16 mA cm^{-2} at -0.40 V), similar to that reported for CN material.[12] Since the G–CN nanosheets and their counterparts (CN nanosheets) obtained by the same metal-free synthesis procedure possess identical microstructures, the significantly enhanced activity of the G–CN nanosheets must be attributed to the incorporation of graphene layers into the nanosheets, which results in enhanced electrical conductivity. This observation can be further confirmed by the electrochemical impedance spectra (EIS) characterization presented in Figure S8 (see the Supporting Information). The overall resistance of G–CN nanosheets is much lower than that of CN nanosheets.

The influence of the pyrolysis temperature on the electrocatalytic properties of G–CN nanosheets is further explored because the pyrolysis temperature can largely affect the amounts of N bonding configurations in G–CN samples (Figure 5c and d). Interestingly, when the pyrolysis temperature is increased from 600 to 1000 °C, the kinetic current density of G–CN nanosheets significantly increases to the highest value of 7.3 mA cm^{-2} at 800 °C and then decreases (Figure 5d). This observation indicates that the electrical conductivity is not the only factor that determines the electrocatalytic activity. According to recent reports,[6a,8a] it has been suggested that the content of nitrogen, especially the pyrindinic or/and graphitic nitrogen portion, is crucial for the promotion of the electrocatalytic reaction in ORR. In association with our XPS analysis of G–CN nanosheets, that is, with the increase of pyrolysis temperature from 800 to 1000 °C, the content of graphitic N is kept constant while that of pyridinic N is largely decreased; therefore it is reasonable to believe that the lower activity of G–CN1000 compared to that of G–CN800 can be attributed to the lower content of pyridinic N in the materials. Given that pyridinic nitrogen atoms with strong electron-accepting ability can create a net positive charge on the adjacent carbon atoms in the G–CN sheets, they are favorable for the adsorption of oxygen atoms and can readily attract electrons from the anode, thus facilitating the ORR.[8a] In addition, the durability of the G–CN for ORR in O_2-saturated 0.1 M KOH solution is evaluated by a chronoamperometric approach. The continuous catalysis (30000 s) at -0.25 V only causes a slight loss of the specific catalytic activity (Figure S9), hence indicating that the catalytic sites in G–CN nanosheets are fairly stable in an alkaline medium.

In summary, we have demonstrated an effective approach for the fabrication of graphene-based carbon nitride nanosheets. The prominent features of these nanosheets including their high nitrogen content, thin thicknesses, high surface areas, and enhanced electrical conductivity, eventually lead to outstanding electrocatalytic activity, long durability, and high selectivity when G–CN nanosheets are employed as metal-free catalysts for ORR. Our studies are the first to reveal that both the electrical conductivity and the content of pyridinic N are two vital factors for achieving high-performance nitrogen-doped carbon materials for ORR since they significantly affect the electron transportation in electrodes and active sites for oxygen reduction. Along with this cost-effective protocol of graphene incorporation, a series of graphene-based nitrogen-enriched carbon materials can be fabricated to broaden their applications across the areas of catalysis, sensors, supercapacitors, and lithium ion batteries.

Received: January 10, 2011
Revised: March 17, 2011
Published online: May 9, 2011

Keywords: carbon nitride · electrocatalysts · fuel cells · graphene · oxygen reduction reaction

[1] a) K. P. Gong, F. Du, Z. H. Xia, M. Durstock, L. M. Dai, *Science* **2009**, *323*, 760; b) W. Xiaog, F. Du, Y. Liu, A. Perez, Jr., M. Supp, T. S. Ramakrishnan, L. M. Dai, L. Jiang, *J. Am. Chem. Soc.* **2010**, *132*, 15839–15841; c) J. Snyder, T. Fujita, M. W. Chen, J. Erlebacher, *Nat. Mater.* **2010**, *9*, 904; M. Lefevre, E. Proietti, F. Jaouen, J. P. Dodelet, *Science* **2009**, *324*, 71.

[2] a) L. T. Qu, Y. Liu, J. B. Baek, L. M. Dai, *ACS Nano* **2010**, *4*, 1321; b) D. S. Yu, E. Nagelli, F. Du, L. M. Dai, *J. Phys. Chem. Lett.* **2010**, *1*, 2165.

[3] J. Zhang, K. Sasaki, E. Sutter, R. R. Adzic, *Science* **2007**, *315*, 220.

[4] R. Bashyam, P. Zelenay, *Nature* **2006**, *443*, 63.

[5] J. P. Collman, N. K. Devaraj, R. A. Decreau, Y. Yang, Y. L. Yan, W. Ebina, T. A. Eberspacher, C. E. D. Chidsey, *Science* **2007**, *315*, 1565.

[6] a) R. L. Liu, D. Q. Wu, X. L. Feng, K. Müllen, *Angew. Chem.* **2010**, *122*, 2619; *Angew. Chem. Int. Ed.* **2010**, *49*, 2565; b) X. Q. Wang, J. S. Lee, Q. Zhu, J. Liu, Y. Wang, S. Dai, *Chem. Mater.* **2010**, *22*, 2178.

[7] a) T. Ikeda, M. Boero, S. F. Huang, K. Terakura, M. Oshima, J. Ozaki, *J. Phys. Chem. C* **2008**, *112*, 14706; b) R. A. Sidik, A. B. Anderson, N. P. Subramanian, S. P. Kumaraguru, B. N. Popov, *J. Phys. Chem. B* **2006**, *110*, 1787.

[8] a) D. S. Yu, Q. Zhang, L. M. Dai, *J. Am. Chem. Soc.* **2010**, *132*, 15127–15129; b) G. Liu, X. G. Li, P. Ganesan, B. N. Popov, *Electrochim. Acta* **2010**, *55*, 2853.

[9] X. C. Wang, K. Maeda, A. Thomas, K. Takanabe, G. Xin, J. M. Carlsson, K. Domen, M. Antonietti, *Nat. Mater.* **2009**, 8, 76.

[10] A. Thomas, A. Fischer, F. Goettmann, M. Antonietti, J. O. Müller, R. Schlögl, J. M. Carlsson, *J. Mater. Chem.* **2008**, *18*, 4893.

[11] a) A. Vinu, K. Ariga, T. Mori, T. Nakanishi, S. Hishita, D. Golberg, Y. Bando, *Adv. Mater.* **2005**, *17*, 1648; b) A. Vinu, P. Srinivasu, D. P. Sawant, T. Mori, K. Ariga, J. S. Chang, S. H. Jhung, V. V. Balasubramanian, Y. K. Hwang, *Chem. Mater.* **2007**, *19*, 4367.

[12] a) S. M. Lyth, Y. Nabae, S. Moriya, S. Kuroki, M. Kakimoto, J. Ozaki, S. Miyata, *J. Phys. Chem. C* **2009**, *113*, 20148; b) Y. Q.

Sun, C. Li, Y. X. Xu, H. Bai, Z. Y. Yao, G. Q. Shi, *Chem. Commun.* **2010**, *46*, 4740.

[13] a) T. O. Wehling, K. S. Novoselov, S. V. Morozov, E. E. Vdovin, M. I. Katsnelson, A. K. Geim, A. I. Lichtenstein, *Nano Lett.* **2008**, *8*, 173; b) S. B. Yang, X. L. Feng, S. Ivanovici, K. Müllen, *Angew. Chem.* **2010**, *122*, 8586; *Angew. Chem. Int. Ed.* **2010**, *49*, 8408; c) S. B. Yang, G. L. Cui, S. P. Pang, Q. Cao, U. Kolb, X. L. Feng, J. Maier, K. Müllen, *ChemSusChem* **2010**, *3*, 236; d) Q. Su, S. P. Pang, V. Alijani, C. Li, X. L. Feng, K. Müllen, *Adv. Mater.* **2009**, *21*, 3191.

[14] M. D. Stoller, S. J. Park, Y. W. Zhu, J. H. An, R. S. Ruoff, *Nano Lett.* **2008**, *8*, 3498.

[15] A. Fasolino, J. H. Los, M. I. Katsnelson, *Nat. Mater.* **2007**, 6, 858.

[16] A. A. Balandin, S. Ghosh, W. Z. Bao, I. Calizo, D. Teweldebrhan, F. Miao, C. N. Lau, *Nano Lett.* **2008**, *8*, 902.

[17] S. B. Yang, X. L. Feng, L. Wang, K. Tang, J. Maier, K. Müllen, *Angew. Chem.* **2010**, *122*, 4905; *Angew. Chem. Int. Ed.* **2010**, *49*, 4795.

[18] W. Chen, S. W. Chen, *Angew. Chem.* **2009**, *121*, 4450; *Angew. Chem. Int. Ed.* **2009**, *48*, 4386.

